A numerical approach to harmonic non-commutative spectral field theory

Bernardino Spisso[1] and Raimar Wulkenhaar[2]

[1,2] *Mathematisches Institut der Westfälischen Wilhelms-Universität*
Einsteinstraße 62, D-48149 Münster, Germany

Abstract

We present a first numerical investigation of a non-commutative gauge theory defined via the spectral action for Moyal space with harmonic propagation. This action is approximated by finite matrices. Using Monte Carlo simulation we study various quantities such as the energy density, the specific heat density and some order parameters, varying the matrix size and the independent parameters of the model. We find a peak structure in the specific heat which might indicate possible phase transitions. However, there are mathematical arguments which show that the limit of infinite matrices can be quite different from the original spectral model.

1   Introduction

Quantum field theory on noncommutative spaces [1, 2, 3] is an active subject of research. The most-studied noncommutative spaces are the Moyal space [4] and fuzzy spaces [5]. Fuzzy spaces are matrix approximations of manifolds and as such ideal for numerical investigations similar to non-perturbative quantum field theory on the lattice. In this paper we focus on the Moyal space, which is a continuous deformation of $\mathbb{R}^d$ for which the usual Fourier techniques of perturbative quantum field theory are available. It turned out that a renormalisable quantum field theory on $\mathbb{R}^d$ is, in most cases, no longer renormalisable on d-dimensional Moyal space due to a phenomenon called ultraviolet/infrared mixing [6]. In [7] it was discovered that for the φ^4-model on 4-dimensional Moyal space the UV/IR-mixing generates an additional marginal coupling which corresponds to a harmonic oscillator potential for the free scalar field. The resulting action

$$S[\varphi] = \int d^4x \left(\frac{1}{2}\varphi \star (-\Delta + \Omega^2 \tilde{x}^2 + \mu^2) \star \varphi + \frac{\lambda}{4}\varphi \star \varphi \star \varphi \star \varphi \right)(x) \tag{1}$$

was then shown to be perturbatively renormalisable to all orders in λ. In (1), $\tilde{x} = 2\Theta^{-1} \cdot x$, where Θ is the deformation matrix defining the Moyal product. See also [8, 9, 10, 11, 12]. Moreover, the frequency parameter can be restricted to $\Omega \in [0,1]$ by Langmann-Szabo duality [13].

---

[1]nispisso@tin.it
[2]raimar@math.uni-muenster.de

The renormalisability of the action (1) raises the question whether a harmonic term can also render Yang-Mills theory renormalisable on Moyal space (recall that the usual Yang-Mills action on Moyal space has the same UV/IR-mixing problem [14]). Yang-Mills theories in noncommutative geometry [15] are naturally obtained from the spectral action principle [16] relative to an appropriate Dirac operator. In [17] it was shown that Moyal space (with usual Dirac operator) is a (non-compact) spectral triple; its corresponding spectral action was computed in [18]. To obtain a gauge theory with harmonic oscillator potential via the spectral action principle, a differential square root of the harmonic oscillator Hamiltonian is necessary as Dirac operator. In absence of such a Dirac operator, in [19, 20] an effective gauge model was constructed as the one-loop effective action of complex harmonic noncommutative quantum φ^4-theory in a classical external gauge field. As a result, the noncommutative Yang-Mills Lagrangian is extended by two terms $X_\mu \star X^\mu$ and $(X_\mu \star X^\mu)^2$, where $X_\mu = \frac{1}{2}\tilde{x}_\mu + A_\mu$ is the 'covariant coordinate'.

A first outline of a candidate spectral triple for harmonic oscillator Moyal space was given in [21]. Additionally, in [21] the linear and quadratic terms of the spectral action for a $U(1)$-Yang-Mills-Higgs model were computed and then extended by gauge invariance. Thereby the appearance of $X_\mu \star X^\mu$ was traced back to a deep entanglement of gauge and Higgs fields in a unified potential $(\alpha X_\mu \star X^\mu + \beta \bar{\varphi} \star \varphi - 1)^2$, with $\alpha, \beta \in \mathbb{R}^+$.

It turned out that the candidate spectral triple proposed in [21] was the shadow of a new class of non-compact spectral triples with finite volume [22]. The spectral geometry of Moyal space with harmonic propagation, which falls into this class, was fully worked out in [23]. There are in fact two (even, real) spectral triples $(\mathcal{A}_\star, \mathcal{H}, \mathcal{D}_\bullet, \Gamma, J)$, with $\bullet \in \{1, 2\}$, for the d-dimensional Moyal algebra $\mathcal{A}_\star$ and differential square roots $\mathcal{D}_\bullet$ of the harmonic oscillator Hamiltonian. The spectral triples are of metric dimension d and KO-dimension $2d$, have simple dimension spectrum consisting of the integers $\leq d$, and satisfy all regularity and compatibility requirements of spectral triples. Additionally, the spectral action was rigorously computed in [23], i.e. with Hölder type estimates for the remainder of the asymptotic expansion and with inclusion of the real structure J.

A completely new feature of the spectral action [23, 21] (and also of the effective action [19, 20]) is that the expansion of $X_\mu \star X^\mu$ and its square produces a term which is *linear in the gauge field A*. This means that the vacuum, i.e. the solution of the classical field equations, is no longer taken at $A_\mu = 0$ (or more generally at a flat connection $F_{\mu\nu} = 0$) but at some non-constant value for the gauge field. A first discussion of the vacuum structure of this type of gauge models was given in [24]. It turned out that generically there are infinitely many vacuum solutions. Some of them were exposed, but it was not possible to give reasonable argument for the right solution. In particular, it became completely impossible to study the gauge model as a perturbative quantum field theory.

This is the point where the numerical treatment comes into play. The standard method of numerical quantum field theory is to approximate the space by discrete points, for example using a lattice approximation and then calculate the observables over that set of points [25]. For Moyal space a position space approximation is not suitable due to the oscillator factor of the Moyal product. Instead, we shall use the matrix Moyal base (which was already used in the first renormalisation proof [7] of φ^4-model), restrict it to finite matrices and perform a Monte Carlo simulation of the resulting action. In this way we will study some statistical quantities such as

energy density and specific heat, varying the parameters $\Omega, \frac{\chi-1}{\chi 0}, \alpha$ of the model and gathering some information on the various contributions of the fields to the action. The simulations are quite cumbersome due the complexity of the action and the number of independent matrices to handle. Nevertheless we are able to get an acceptable balance between the computation precision and the computation time. For the simulations we apply a standard Metropolis-Monte Carlo algorithm [26] with various estimators for the error and for the autocorrelation time of the samples. The range of parameters is chosen to avoid problems with the thermalisation process, thus permitting a relative small number of Monte Carlo steps to compute independent results from the initial conditions.

We are eventually interested in the continuum limit which corresponds to matrices of infinite size. We thus compute our observables such as the energy density for various matrix sizes and then look for a stabilization of these observables as the matrix size increases. The specific heat, which is a measure of the dispersion of the energy, will be used to identify possible phase transitions in form of peaks of the specific heat at increasing matrix size.

2   Four-dimensional harmonic Yang-Mills model

The harmonic Yang-Mills model is defined as the spectral action resulting from the spectral triples $(\mathcal{A}_\star, \mathcal{H}, \mathcal{D}_\bullet, \Gamma, J)$, with $\bullet \in \{1, 2\}$, analysed in [23]. The Moyal algebra $\mathcal{A}_\star$ is the space of Schwartz class functions on $\mathbb{R}^4$ equipped with the product

$$f \star g(x) = \int_{\mathbb{R}^4 \times \mathbb{R}^4} \frac{dy\, dk}{(2\pi)^4} \, f(x+\tfrac{1}{2}\Theta \cdot k)\, g(x+y)\, \mathrm{e}^{i\langle k, y\rangle} \ . \tag{2}$$

Where $\langle k, y\rangle$ is the scalar product defined as $k_\mu y^\mu$. The unbounded selfadjoint operators $\mathcal{D}_\bullet$ on the Hilbert space $\mathcal{H}$ are differential square roots of the harmonic oscillator Hamiltonian $H = -\partial_\mu \partial^\mu + \tilde{\Omega}^2 x_\mu x^\mu$ of frequency $\tilde{\Omega}$, i.e. $\mathcal{D}_\bullet^2 = H - (-1)^\bullet \tilde{\Omega}\Sigma$, for a certain spin matrix Σ. If $L_\star(f)$ denotes left Moyal multiplication with a function $f \in \mathcal{A}_\star$, then one has

$$[\mathcal{D}_1, L_\star(f)] = L_\star(i\partial_\mu f) \otimes \Gamma^\mu \ , \qquad\qquad [\mathcal{D}_2, L_\star(f)] = L_\star(i\partial_\mu f) \otimes \Gamma^{\mu+4} \ , \tag{3}$$

where the matrices $\Gamma_1, \ldots, \Gamma_8$ satisfy the anticommutation relations

$$\{\Gamma^\mu, \Gamma^\nu\} = \{\Gamma^{\mu+4}, \Gamma^{\nu+4}\} = 2(g^{-1})^{\mu\nu} \ , \quad \{\Gamma^\mu, \Gamma^{\nu+4}\} = 0 \ , \tag{4}$$

relative to an induced metric $g = (\mathrm{id} - \tfrac{1}{4}\tilde{\Omega}^2\Theta^2)^{-1}$. The grading is $\Gamma = \Gamma_1 \cdots \Gamma_8$, and the real structure satisfy $J\mathcal{D}_\bullet J^{-1} = \mathcal{D}_\bullet$ and $JL_\star(f)J^{-1} = R_\star(\bar{f})$, where $R_\star$ denotes right Moyal multiplication.

In order to implement the Higgs mechanism à la Connes-Lott [27] one considers the product of the spectral triple $(\mathcal{A}_\star, \mathcal{H}, \mathcal{D}_1, \Gamma, J)$ with the finite Higgs spectral triple $(\mathbb{C} \oplus \mathbb{C}, \mathbb{C}^2, M\sigma_1, J_f)$, where σ_1 is a Pauli matrix, J_f any matricial real structure and $M > 0$. Then, a self-adjoint fluctuation $A = \sum a_i[\mathcal{D}, b_i]$ of the total Dirac operator $\mathcal{D} = (\mathcal{D}_1 \otimes 1 + \Gamma \otimes M\sigma_1)$ to give $\mathcal{D}_A = \mathcal{D} + A + \mathrm{J}A\mathrm{J}^{-1}$, for $\mathrm{J} = J \otimes J_f$, is of the form

$$A = \begin{pmatrix} \Gamma^\mu L_\star(A_\mu) & \Gamma L_\star(\phi) \\ \Gamma L_\star(\bar{\phi}) & \Gamma^\mu L_\star(B_\mu) \end{pmatrix} \ , \tag{5}$$

3

for the components $A_\mu, B_\mu \in \mathcal{A}_\star$ of two real one-forms and a complex scalar $\phi \in \mathcal{A}_\star$. Using $\mathcal{D}_2$ instead of $\mathcal{D}_1$ amounts to replace Γ^μ by $\Gamma^{\mu+4}$.

The spectral action principle [16] asserts that the bosonic action of a field theory with fermionic Dirac operator $\mathcal{D}_A$ has the form

$$S(\mathcal{D}_A) = \mathrm{Tr}(\chi(\mathcal{D}_A^2)) \,, \tag{6}$$

where χ is a smooth approximation of the characteristic function on $[0, \Lambda^2]$, for some scale parameter Λ. For the fluctuation (5), the part of the spectral action which is relevant and marginal for $\Lambda \to \infty$ has been explicitly computed in [23], for general effective metric g. This computation involved Laplace transformation, Duhamel expansion with Hölder-type estimates for the remainder and explicit use of the Mehler kernel for the harmonic oscillator Hamiltonian. For a special choice of the noncommutativity matrix $\Theta^2 = -\theta^2 \mathrm{id}$, the result of [23] takes in terms of $\Omega := \frac{\theta\tilde\Omega}{2}$, the moments $\Lambda^{2n}\chi_{-n} := \int_0^\infty ds\, s^{n-1}\chi(s)$ of the "characteristic function" and $\chi_0 := \chi(0)$ the form

$$S_\Lambda(\mathcal{D}_A) = \frac{\theta^4\Lambda^8}{8\Omega^4}\chi_{-4} - \frac{M^2\theta^4\Lambda^6}{8\Omega^4}\chi_{-3} + \Big(\frac{M^4\theta^4\Lambda^4}{16\Omega^4} + \frac{8\theta^2\Lambda^4}{12\Omega^2}\Big)\chi_{-2} - \Big(\frac{M^6\theta^4\Lambda^2}{48\Omega^4} + \frac{2M^2\theta^2\Lambda^2}{3\Omega^2}\Big)\chi_{-1}$$

$$+ \Big(\frac{52}{45} + \frac{M^8\theta^4}{192\Omega^4} + \frac{M^4\theta^2}{3\Omega^2}\Big)\chi_0$$

$$+ \frac{\chi_0}{\pi^2(1+\Omega^2)^2}\int d^4x \Big\{ 2(1+\Omega^2)D_\mu\phi \star \overline{D^\mu\phi}$$

$$+ \Big(\phi\star\bar\phi + M(\phi+\bar\phi) + \frac{4\Omega^2}{1+\Omega^2}\tilde{X}_{A\mu}\star\tilde{X}_A^\mu + M^2 - \frac{\chi_{-1}}{\chi_0}\Lambda^2\Big)^2 - \Big(\frac{4\Omega^2}{1+\Omega^2}\tilde{X}_{0\mu}\star\tilde{X}_0^\mu + M^2 - \frac{\chi_{-1}}{\chi_0}\Lambda^2\Big)^2$$

$$+ \Big(\bar\phi\star\phi + M(\phi+\bar\phi) + \frac{4\Omega^2}{1+\Omega^2}\tilde{X}_{B\mu}\star\tilde{X}_B^\mu + M^2 - \frac{\chi_{-1}}{\chi_0}\Lambda^2\Big)^2 - \Big(\frac{4\Omega^2}{1+\Omega^2}\tilde{X}_{0\mu}\star\tilde{X}_0^\mu + M^2 - \frac{\chi_{-1}}{\chi_0}\Lambda^2\Big)^2$$

$$+ \Big(\frac{(1+\Omega^2)^2}{2} - \frac{(1-\Omega^2)^4}{6(1+\Omega^2)^2}\Big)\big(F_{\mu\nu}^A \star F^{A\mu\nu} + F_{\mu\nu}^B \star F^{B\mu\nu}\big) \Big\}$$

$$+ \mathcal{O}(\Lambda^{-1}) \,. \tag{7}$$

Here, $D_\mu\phi = \partial_\mu\phi - iA_\mu \star \phi + i\phi \star B_\mu - iM(A_\mu - B_\mu)$ is the covariant derivative of the scalar field, $F_{\mu\nu}^A := \partial_\mu A_\nu - \partial_\nu A_\mu - i(A_\mu \star A_\nu - A_\nu \star A_\mu)$ the field strength of A and similarly $F_{\mu\nu}^B$ the field strength of B. Moreover, $\tilde{X}_{A\mu} := \tilde{X}_{0\mu} + A_\mu$ and $\tilde{X}_{B\mu} := \tilde{X}_{0\mu} + B_\mu$ are the covariant derivatives of A and B, respectively, where $\tilde{X}_{0\mu} := \frac{\tilde{x}_\mu}{2} = (\Theta^{-1})_{\mu\nu}x^\nu$. The remarkable outcome of the spectral action (7) is that the Higgs field ϕ *and* the gauge fields A, B appear together in a unified potential. In this way, also the gauge field shows a non-trivial vacuum structure. Besides, the action is invariant under $U(\mathcal{A}_\star) \times U(\mathcal{A}_\star)$ transformations:

$$(\phi + M) \mapsto u_A \star (\phi + M) \star \overline{u_B}, \quad \tilde{X}_\mu^A \mapsto u_A \star \tilde{X}_A^\mu \star \overline{u_A}, \quad \tilde{X}_B^\mu \mapsto u_B \star \tilde{X}_B^\mu \star \overline{u_B} \,. \tag{8}$$

3   Discretisation by Moyal base

The 2-dimensional Moyal algebra with deformation parameter $\theta > 0$ has a natural basis of eigenfunctions f_{mn} of the harmonic oscillator, where $m, n \in \mathbb{N}$. These are given in radial coordinates by

$$f_{mn}(\rho\cos\varphi, \rho\sin\varphi) = 2(-1)^m\sqrt{\frac{m!}{n!}}e^{i\varphi(n-m)}\Big(\sqrt{\frac{2}{\theta}}\rho\Big)^{n-m}e^{-\frac{\rho^2}{\theta}}L_m^{n-m}\Big(\frac{2}{\theta}\rho^2\Big) \tag{9}$$

and satisfy

$$(f_{mn} \star f_{kl})(x) = \delta_{nk} f_{ml}(x) \tag{10}$$

$$\int d^2x \, f_{mn}(x) = 2\pi\theta\delta_{mn} \, , \tag{11}$$

see [4, 17] for details. The expansion of Schwartz functions on $\mathbb{R}^4$ in the Moyal base,

$$\mathcal{A}_\star \ni a = a(x_0, \ldots, x_3) = \sum_{m_1, m_2, n_1, n_2 \in \mathbb{N}} a_{\substack{m_1 n_1 \\ m_2 n_2}} f_{m_1 n_1}(x_0, x_1) f_{m_2 n_2}(x_2, x_3) \, , \tag{12}$$

then provides an isomorphism of Fréchet spaces between $\mathcal{A}_\star$ and the space of rapidly decreasing double sequences $(a_{mn})_{m,n \in \mathbb{N}^2}$ equipped with the family of seminorms

$$p_k((a_{mn})_{m,n \in \mathbb{N}^2}) := \sum_{m,n \in \mathbb{N}^2}^{\infty} \left((2|m|+1)^{2k}(2|n|+1)^{2k}|a_{mn}|^2 \right)^{\frac{1}{2}} \, , \qquad |m| := m_1 + m_2 \, . \tag{13}$$

According to (10), Moyal product and integral reduce in the (f_{mn})-basis to product and trace of infinite $\mathbb{N}^2$-labeled matrices, with convergent index sums due to (13). By duality, the covariant derivatives X_μ^A and X_μ^B can also be expanded in the (f_{mn})-basis, but the expansion coefficients $X_{\mu \substack{m_1 n_1 \\ m_2 n_2}}^A$, $X_{\mu \substack{m_1 n_1 \\ m_2 n_2}}^B$ diverge for $m_i, n_i \to \infty$.

To any $a \in \mathcal{A}_\star$ we can associate a sequence $(a^N)_{N \in \mathbb{N}}$ of cut-off matrices

$$a^N_{\substack{m_1 n_1 \\ m_2 n_2}} = \begin{cases} a_{\substack{m_1 n_1 \\ m_2 n_2}} & \text{if } \max(m_1, m_2, n_1, n_2) \leq N \, , \\ 0 & \text{else} \, . \end{cases}$$

Then, (a^N) is a Cauchy sequence in any of the semi-norms p_k and converges to a in the Fréchet topology of $\mathcal{A}_\star$.

In quantum field theory we are confronted with the converse problem. To deal with divergences, a regularisation has to be introduced which restricts the system to a finite number of degrees of freedom. After re-normalisation from bare to physical quantities one has to show that the limit to an infinite number of degrees of freedom is well-defined. In our case, the natural regularisation is to restrict the matrix indices to $m_i \leq N$, which corresponds to a cut-off in the energy. Even if we could solve the renormalisation problem, the removal of the cut-off, i.e. the limit $N \to \infty$ to infinite matrices, will fail: A sequence of $(N \times N)$-matrix algebras does not converge in the Fréchet topology.

Fortunately, in quantum field theory we are interested in the convergence of correlation functions, and not of matrix algebras. The path integral in usual quantum field theories is over random walks and not over smooth field configurations. It seems not impossible (although we cannot prove it) that quantum correlation functions are less sensitive to the topology of the underlying classical field theory. In our case, we make the (not verifiable) hypothesis that the cut-off correlation functions to be computed carry some information about the original smooth model.

Using the identities $D_\mu\phi = i(\phi+M)\star\tilde{X}_{B\mu} - i\tilde{X}_{A\mu}\star(\phi+M)$ and $F_{\mu\nu}^A = -i[X_\mu^A, X_\nu^A] + i[X_\mu^0, X_\nu^0]$ (and similarly for $F_{\mu\nu}^B$), and ignoring all contributions of X_μ^0 which for finite matrices yields some

finite number, we can recast the restriction of the action (7) to finite matrices in the following form:

$$
\begin{aligned}
S(\phi, \tilde{X}_A, \tilde{X}_B) = \frac{1}{(1+\Omega^2)^2} \mathrm{Tr}\Bigg\{ & \left(\frac{(1-\Omega^2)^2}{2} - \frac{(1+\Omega^2)^4}{6\,(1+\Omega^2)^2} \right) \left(\left[\tilde{X}_{A\mu}, \tilde{X}_{A\nu} \right]_\star \left[\tilde{X}_A^\mu, \tilde{X}_A^\nu \right]_\star \right. \\
& \left. + \left[\tilde{X}_{B\mu}, \tilde{X}_{B\nu} \right]_\star \left[\tilde{X}_B^\mu, \tilde{X}_B^\nu \right]_\star \right) \\
& + \left(\phi \star \bar{\phi} + M(\phi + \bar{\phi}) + \frac{4\Omega^2}{1+\Omega^2} \tilde{X}_A^\mu \star \tilde{X}_{A\mu} + M^2 - \Lambda^2 \frac{\chi_{-1}}{\chi_0} \right)^2 \\
& + \left(\bar{\phi} \star \phi + M(\phi + \bar{\phi}) + \frac{4\Omega^2}{1+\Omega^2} \tilde{X}_B^\mu \star \tilde{X}_{B\mu} + M^2 - \Lambda^2 \frac{\chi_{-1}}{\chi_0} \right)^2 \\
& + 2(1 + \Omega^2) \left((\phi + M) \star \tilde{X}_{B\mu} - \tilde{X}_{A\mu} \star (\phi + M) \right) \\
& \left((\bar{\phi} + M) \star \tilde{X}_A^\mu - \tilde{X}_B^\mu \star (\bar{\phi} + M) \right) \Bigg\} .
\end{aligned}
\tag{14}
$$

The restriction to finite matrices shows crucial differences to the smooth model. Only these differences make the numerical simulations possible with the drawback of the serious possibility that our results can deviate from the original smooth model.

1. The action (14) has an obvious family of minima given appropriate multiples of the identity matrices. We thus define

$$
\phi + M = \psi + \Lambda \sqrt{\frac{\chi_{-1}}{\chi_0}} \cos \alpha \mathbf{I}
\tag{15}
$$

$$
\tilde{X}_{A\mu} = Y_{A\mu} + \frac{1}{2} \Lambda \sqrt{\frac{\chi_{-1}}{\chi_0}} \sqrt{\frac{2\Omega^2}{(1+\Omega^2)}} \mathbf{I}_\mu \sin \alpha
\tag{16}
$$

$$
\tilde{X}_{B\mu} = Y_{B\mu} + \frac{1}{2} \Lambda \sqrt{\frac{\chi_{-1}}{\chi_0}} \sqrt{\frac{2\Omega^2}{(1+\Omega^2)}} \mathbf{I}_\mu \sin \alpha \ .
\tag{17}
$$

Note that the corresponding minimum configurations for A_μ, B_μ explicitly violate, in the limit $N \to \infty$, the Fréchet condition.

Substituting the previous fields into (14) we get a positive action with minimum in zero:

$$
\begin{aligned}
S(\psi, Y_A, Y_B) = \frac{1}{(1+\Omega^2)^2} \mathrm{Tr}\Bigg\{ & D\Big([Y_{A\mu}, Y_{A\nu}] \left[Y_A^\mu, Y_A^\nu \right] + [Y_{B\mu}, Y_{B\nu}] \left[Y_B^\mu, Y_B^\nu \right] \Big) \\
& + \left(\psi \bar{\psi} + \mu \cos \alpha (\psi + \bar{\psi}) + C Y_A^\mu Y_{A\mu} + \mu \mathbf{I}^\mu Y_{A\mu} \sin \alpha \right)^2 \\
& + \left(\bar{\psi} \psi + \mu \cos \alpha (\psi + \bar{\psi}) + C Y_B^\mu Y_{B\mu} + \mu \mathbf{I}^\mu Y_{B\mu} \sin \alpha \right)^2 \\
& + 2(1 + \Omega^2) \left((Y_{B\mu} - Y_{A\mu}) \mu \cos \alpha + \psi Y_{B\mu} - Y_{A\mu} \psi \right) \\
& \left((Y_A^\mu - Y_B^\mu) \mu \cos \alpha + \bar{\psi} Y_A^\mu - Y_B^\mu \bar{\psi} \right) \Bigg\},
\end{aligned}
\tag{18}
$$

with

$$
C = \frac{1+\Omega^2}{4\Omega^2} \ , \qquad D = \frac{(1-\Omega^2)^2}{2} - \frac{(1+\Omega^2)^4}{6\,(1+\Omega^2)^2} \ , \qquad \Lambda^2 \frac{\chi_{-1}}{\chi_0} = \mu^2 \ .
\tag{19}
$$

6

2. For finite matrices, the $\mathbb{N}^2$-indexed double sequences can be written as tensor products of ordinary matrices,

$$X_{\substack{m_1 n_1 \\ m_2 n_2}} = \sum_{i=1}^{K} X^i_{m_1 n_1} \otimes X^i_{m_2 n_2} . \tag{20}$$

Since the matrix product and trace also factor into these independent components, the action factors into $S = \sum_{i=1}^{K} S(\psi^{1i}, Y_A^{1i}, Y_B^{1i}) S(\psi^{2i}, Y_A^{2i}, Y_B^{2i})$. Then, regarding all ψ^{1i}, Y_A^{1i}, $Y_B^{1i}, \psi^{2i}, Y_A^{2i}, Y_B^{2i}$ as random variables over which to integrate in the partition function, the partition function factors, too:

$$\int \mathcal{D}(\psi^{11}, Y_A^{11}, Y_B^{11}, \psi^{21}, Y_A^{21}, Y_B^{21}) \cdots \mathcal{D}(\psi^{1K}, Y_A^{1K}, Y_B^{1K}, \psi^{2K}, Y_A^{2K}, Y_B^{2K}) \, e^{-S}$$

$$= \left(\int \mathcal{D}(\psi^{1i}, Y_A^{1i}, Y_B^{1i}, \psi^{2i}, Y_A^{2i}, Y_B^{2i}) \, e^{-S(\psi^{1i}, Y_A^{1i}, Y_B^{1i}) \cdot S(\psi^{2i}, Y_A^{2i}, Y_B^{2i})} \right)^K . \tag{21}$$

We may therefore restrict ourselves to $K = 1$. Now the discretized action is invariant under the same transformations (8), but now with $(u_A, u_B) \in U(\mathbb{M}_N) \times U(\mathbb{M}_N)$. For the limit $N \to \infty$ we would have $K \to \infty$ and therefore problems with convergence.

3. Instead of integrating in the partition function over all gauge-equivalence classes of ψ, Y_A, Y_B as required, we follow the usual matrix model philosophy[1] and integrate over *all* matrices ψ, Y_A, Y_B. A reduction of this 10-matrix model to gauge-equivalence classes seems rather hopeless.

It is convenient to pass, for each factor in the tensor product (20), to complex matrices [24]:

$$
\begin{aligned}
Z_0 &= Y_0^A + iY_1^A, & \bar{Z}_0 &= Y_0^A - iY_1^A \\
Z_1 &= Y_0^B + iY_1^B, & \bar{Z}_1 &= Y_0^B - iY_1^B \\
Z_2 &= Y_2^A + iY_2^A, & \bar{Z}_2 &= Y_2^A - iY_3^A \\
Z_3 &= Y_2^B + iY_3^B, & \bar{Z}_3 &= Y_2^B - iY_3^B
\end{aligned}
\tag{22}
$$

The convention that the bar denotes the hermitian conjugate will also be used for the complex matrix ψ. In the end using the substitutions (22) and after some simple manipulations, the discretised action is:

$$S_4 = \frac{1}{(1 + \Omega^2)} \operatorname{Tr} \left(\mathcal{L}_F + \mathcal{L}_{V_0} + \mathcal{L}_{V_1} + \mathcal{L}_{D_0} \bar{\mathcal{L}}_{D_0} + \mathcal{L}_{D_1} \bar{\mathcal{L}}_{D_1} + \mathcal{L}_{D_2} \bar{\mathcal{L}}_{D_2} + \mathcal{L}_{D_3} \bar{\mathcal{L}}_{D_3} \right) , \tag{23}$$

with

$$
\begin{aligned}
\mathcal{L}_F = \frac{D}{2} \Big(&\big[\bar{Z}_0, Z_0 \big]^2 + \big[\bar{Z}_1, Z_1 \big]^2 + \frac{1}{4} \Big(\big[Z_0 + \bar{Z}_0, Z_2 - \bar{Z}_2 \big]^2 - \big[Z_0 + \bar{Z}_0, Z_2 + \bar{Z}_2 \big]^2 \\
&+ \big[Z_0 - \bar{Z}_0, Z_2 + \bar{Z}_2 \big]^2 - \big[Z_0 - \bar{Z}_0, Z_2 - \bar{Z}_2 \big]^2 - \big[Z_1 + \bar{Z}_1, Z_3 + \bar{Z}_3 \big]^2 \\
&+ \big[Z_1 + \bar{Z}_1, Z_3 - \bar{Z}_3 \big]^2 + \big[Z_1 - \bar{Z}_1, Z_3 + \bar{Z}_3 \big]^2 - \big[Z_1 - \bar{Z}_1, Z_3 - \bar{Z}_3 \big]^2 \Big) \Big)
\end{aligned}
$$

---

[1] In scalar 1-matrix models the gauge-equivalence classes are the configurations of eigenvalues. Nevertheless it is custom to integrate over *all* matrices. The integration over the gauge group produces a measure for the eigenvalues which is given by the square of the Vandermonde determinant. In 2-matrix models the gauge equivalence classes are the eivenvalues together with a unitary matrix which describes the relative orientation of the eigenbases. The full matrix integration can be reduced to an integration over the eingenvalues thanks to the formula of Itzykson-Zuber and Harish-Chandra.

$$\mathcal{L}_{V_0} = \left(\psi\bar{\psi} + \mu\cos\alpha(\psi + \bar{\psi}) + \frac{1}{2}\left(\{\bar{Z}_0, Z_0\} + \{\bar{Z}_2, Z_2\}\right)\right.$$
$$\left. + \frac{\mu\sin\alpha}{2\sqrt{C}}((-1+i)(Z_0 + Z_2) + (1+i)(\bar{Z}_0 + \bar{Z}_2))\right)^2$$
$$\mathcal{L}_{V_1} = \left(\bar{\psi}\psi + \mu\cos\alpha(\psi + \bar{\psi}) + \frac{1}{2}\left(\{\bar{Z}_1, Z_1\} + \{\bar{Z}_3, Z_3\}\right)\right.$$
$$\left. + \frac{\mu\sin\alpha}{2\sqrt{C}}((-1+i)(Z_1 + Z_3) + (1+i)(\bar{Z}_1 + \bar{Z}_3))\right)^2$$
$$\mathcal{L}_{D_0} = \sqrt{2(1+\Omega^2)}\left(\mu\cos\alpha(Z_1 + \bar{Z}_1 - Z_0 - \bar{Z}_0) + \psi(Z_1 + \bar{Z}_1) - (Z_0 + \bar{Z}_0)\psi\right)$$
$$\mathcal{L}_{D_1} = \sqrt{2(1+\Omega^2)}\left(\mu\cos\alpha(Z_1 - \bar{Z}_1 - Z_0 + \bar{Z}_0) + \psi(Z_1 - \bar{Z}_1) - (Z_0 - \bar{Z}_0)\psi\right)$$
$$\mathcal{L}_{D_2} = \sqrt{2(1+\Omega^2)}\left(\mu\cos\alpha(Z_3 + \bar{Z}_3 - Z_2 - \bar{Z}_2) + \psi(Z_3 + \bar{Z}_3) - (Z_2 + \bar{Z}_2)\psi\right)$$
$$\mathcal{L}_{D_3} = \sqrt{2(1+\Omega^2)}\left(\mu\cos\alpha(Z_3 - \bar{Z}_1 - Z_2 + \bar{Z}_2) + \psi(Z_3 - \bar{Z}_3) - (Z_2 - \bar{Z}_2)\psi\right)$$

In this case, (23) becomes an action for 5 complex matrices. For the partition function we need the independent product of two copies of (23), i.e. we are dealing with a complex 10-matrix model. This is already cumbersome and shows that there is little hope to treat the original model (7) where the simplifying consequences of finite matrices are not available.

The next step is to define the estimator for the average values of interest and to specify some numerical parameters in order to analyse the numerical results.

4   Definition of the observables

Following Monte Carlo methods, we will produce a sequence of configurations $\{(\psi, Z_i)_j\}_{j=1,2,\cdots,T_{MC}}$ and evaluate the average of the observables over that set of configurations. These sequences of configurations, called Monte Carlo chain, are representatives of the configuration space at given parameters. In this framework the expectation value is approximated as

$$\langle O \rangle \approx \frac{1}{T_{MC}} \sum_{j=1}^{T_{MC}} O_j \,, \tag{24}$$

where O_j is the value of the observable O evaluated in the j-sampled configuration, $(\psi, Z_i)_j$, $O_j = O[(\psi, Z_i)_j]$. The internal energy is defined as

$$E(\Omega, \mu, \alpha) = \langle S \rangle \,, \tag{25}$$

and the specific heat takes the form

$$C(\Omega, \mu, \alpha) = \langle S^2 \rangle - \langle S \rangle^2 \,. \tag{26}$$

These quantities correspond to the usual definitions for energy

$$E(\Omega, \mu, \alpha) = -\frac{1}{\mathcal{Z}}\frac{\partial \mathcal{Z}}{\partial \beta} \tag{27}$$

and specific heat

$$C(\Omega, \mu, \alpha) = \frac{\partial E}{\partial \beta} \,, \tag{28}$$

8

where $\mathcal{Z}$ is the partition function. It is very useful to compute separately the average values of the four contributions:

$$F(\Omega, \mu, \alpha) = \langle \operatorname{Tr} \mathcal{L}_F \rangle \,, \tag{29}$$

$$V_0(\Omega, \mu, \alpha) = \langle \operatorname{Tr} \mathcal{L}_{V_0} \rangle \,, \tag{30}$$

$$V_1(\Omega, \mu, \alpha) = \langle \operatorname{Tr} \mathcal{L}_{V_1} \rangle \,, \tag{31}$$

$$D(\Omega, \mu, \alpha) = \langle \operatorname{Tr} \left(\mathcal{L}_{D_0} \bar{\mathcal{L}}_{D_0} + \cdots + \mathcal{L}_{D_3} \bar{\mathcal{L}}_{D_3} \right) \rangle \,. \tag{32}$$

4.1 Order parameters

The previous quantities are not enough if we want to measure the various contributions of different modes of the fields to the configuration (ψ, Z_i). Therefore, we need some control parameters usually called order parameters. As a first idea we can think about a quantity related to the norms of the fields, for example the sums $\sum_{nm} |\psi_{nm}|^2$, $\sum_{nm} |Z_{inm}|^2$. These quantities are called the full-power-of-the-field [28, 29]; they can be computed as the trace of the square:

$$\varphi_a^2 = \operatorname{Tr}(|\psi|^2) \tag{33}$$

$$Z_{ia}^2 = \operatorname{Tr}(|Z_i|^2) \tag{34}$$

In contrast, $\langle \varphi_a \rangle$ alone is not a good order parameter because it does not distinguish contributions from the different modes. But we can use it as a reference to define the quantities

$$\varphi_0^2 = \sum_{n=0}^{N} |a_{nn}|^2 \,,$$

$$Z_{i0}^2 = \sum_{n=0}^{N} |z_{inn}|^2 \,, \tag{35}$$

where a_{mn} and z_{imn} are the expansion coefficients of ψ and Z_i, respectively, in the matrix base (9) . Referring to (9) it is easy to see that these parameters (35) are connected with the purely spherical contribution. These quantities will be used to analyse the spherical contribution to the full-power-of-the-field. We can generalise the previous quantity and define parameters φ_l in such a way that they form a decomposition of the full-power-of-the-fields:

$$\varphi_a^2 = \varphi_0^2 + \sum_{l>0} \varphi_l^2, \qquad Z_{ia}^2 = Z_{i0}^2 + \sum_{l>0} Z_{il}^2 \,. \tag{36}$$

Following this prescription, the other quantities for $l > 0$ can be defined as:

$$\varphi_l^2 = \sum_{n,m=0}^{l} |a_{nm}(1 - \delta_{nm})|^2, \qquad Z_{il}^2 = \sum_{n,m=0}^{l} |z_{lnm}(1 - \delta_{nm})|^2 \,. \tag{37}$$

If the contribution is dominated by the spherically symmetric parameter we expect to have $\langle \varphi_a^2 \rangle \sim \langle \varphi_0^2 \rangle$, $\langle Z_{ia}^2 \rangle \sim \langle Z_{i0}^2 \rangle$.

In the next simulations we will evaluate, apart from $l = 0$, the quantity with $l = 1$ as representatives of those contributions where the rotational symmetry is broken. According to (37) we have

$$\varphi_1^2 = |a_{10}|^2 + |a_{01}|^2, \ Z_{i1}^2 = |z_{i10}|^2 + |z_{i01}|^2 \,. \tag{38}$$

9

Using higher l in (37) we could analyse the contributions of the remaining modes, but it turns out that the measurements of the first two modes are enough to characterise the behaviour of the system.

5   Numerical results

Now we discuss the results of the Monte Carlo simulation of the approximated spectral model. As a first approach we use some restrictions on the parameters. Starting point is the approximation (23) of the spectral action. Since (23) is symmetric under the transformation $\mu \mapsto -\mu$ we can assume $\mu \geq 0$ and $\mu^2 \geq 0$. In this first treatment we explore the range $\mu \in [0, 3.1]$, which is enough to show a particular behaviour of the system for fixed Ω. The parameter Ω appears only with its square and is defined as a real parameter, therefore also for Ω we require $\Omega \geq 0$. For the scalar model [7] it was possible to restrict to $\Omega \in [0, 1]$, because Langmann-Szabo duality maps Ω to $\frac{1}{\Omega}$. In the gauge model under consideration, Langmann-Szabo duality is not realised. Due to the prefactor in front of the integral (23), the action vanishes for $\Omega \to \infty$. Studying the plots for the energy and the specific heat, we have chosen the range $\Omega \in [0, 2\pi]$ in which the action is significantly different from zero. The last parameter to consider is α, which is connected to the choice of the vacuum state, with range $\alpha \in [0, 2\pi]$. The study of the system varying α is quite important from a theoretical point of view because it is related to the vacuum invariance. In the action there appear some contributions proportional to $(\sin \alpha)/\Omega$ which seem to diverge for $\Omega = 0$. Numerically we have verified that this is an eliminable divergence and the curves of the observables can be extended to $\Omega = 0$ by continuity. Studying the dependence on α we can conclude that in the limit $N \to \infty$ the observables are independent from α, therefore for our purposes α will be fixed equal to zero avoiding the annoying terms. In general, for each observable we compute the plots for matrix size approximations $N =$ 5, 10, 15, 20.

5.1   Varying α

We start looking at the variation of the energy density and of the full-power-of-the-fields density for fixed μ and Ω, varying $\alpha \in [0, 2\pi]$. As representatives we present the plots for $\mu = 1$, $\Omega \in \{1, 0.5\}$, but we obtain the same behaviour for any other choice of the parameters allowed in the considered range. All three plots show an oscillating behaviour of the values, and this
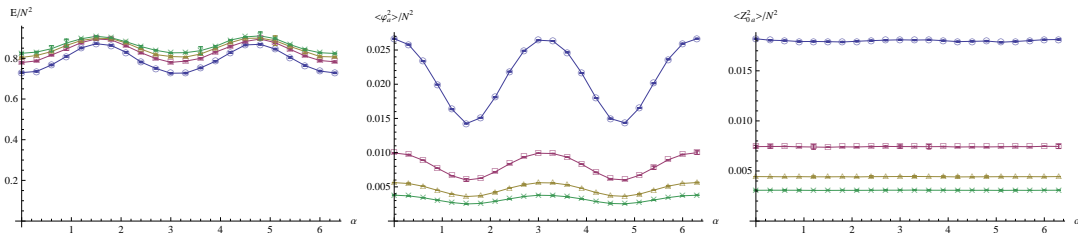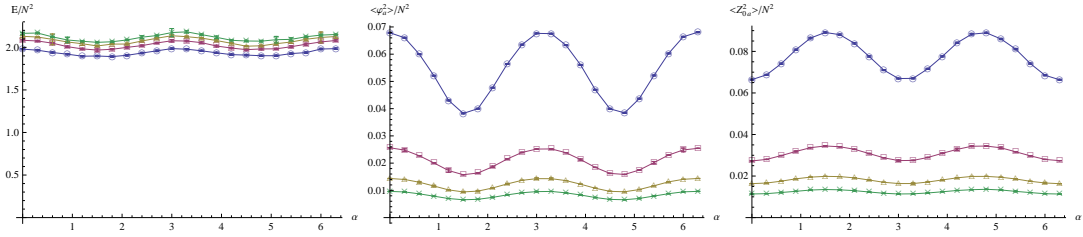

Figure 1: Total energy density and full-power-of-the-fields density for $\langle \varphi_a^2 \rangle$, $\langle Z_{0a}^2 \rangle$ (from the left to the right) fixing $\mu = 1$, $\Omega = 1$, varying α and N. $N = 5$ (circle), $N = 10$ (square), $N = 15$ (triangle), $N = 20$ (cross).

oscillation is present in all other quantities measured. The amplitude of this oscillation becomes

smaller and smaller increasing the size of the matrix and this is true for all the quantities. The same trend is described in fig.2 which shows different positions of the maxima, but again smaller amplitudes for increasing N. These results allow us to consider $\alpha = 0$ for all next plots, since we

Figure 2: Total energy density and full-power-of-the-fields density for $\langle \varphi_a^2 \rangle$, $\langle Z_{0a}^2 \rangle$ (from the left to the right) fixing $\mu = 1$, $\Omega = 0.5$, varying α and N.

are interested in the behaviour of the system for $N \to \infty$. This occurrence simplify all the next simulations thanks to the vanishing of terms $\sim (\sin \alpha)/\Omega$ appearing in the discretised action.

5.2   Varying Ω

As already mentioned we chose $[0,3]$ as range for Ω. In fact, if we look at the plots in fig.3 of the total energy density $\langle S \rangle / N^2$ for $\mu \in \{0, 1\}$, we notice that the action tends to zero for Ω outside the selected interval. This behaviour of the action is the same for all possible choices of parameters and for the specific heat, too.
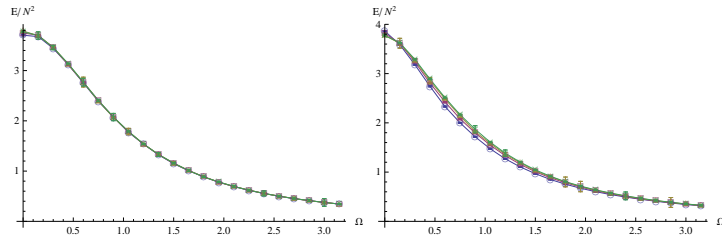
Figure 3: Total energy density and the various contributions for $\mu = 0$ (left), $\mu = 0$ (right), $\alpha = 0$ varying Ω and N. With $N = 5$ (circle), $N = 10$ (square), $N = 15$ (triangle), $N = 20$ (cross).

In the rest of this section we ignore for the computations of $\langle E \rangle, \langle D \rangle, \langle V \rangle, \langle F \rangle$ the global prefactor $(1 + \Omega^2)^{-1}$. In this way we focus our attention to the integral as the source of possible phase transitions. Now we will analyse three cases in which μ is fixed to $0, 1, 3$. In all cases α is zero and we vary $\Omega \in [0, 3]$. The plots in fig.4 show the total energy density and the various contributions: the potential V/N^2, the Yang-Mills part F/N^2 and the covariant derivative part D/N^2, for $\mu = 1$. There is no evident discontinuity or peak, and increasing the size of the matrices the curves remain smooth.

Comparing the energy density and the various contributions in fig.5 we notice that the contributions between F and V balance each other and the total energy follows the slope of D, and this behaviour continues increasing the size of the matrices.
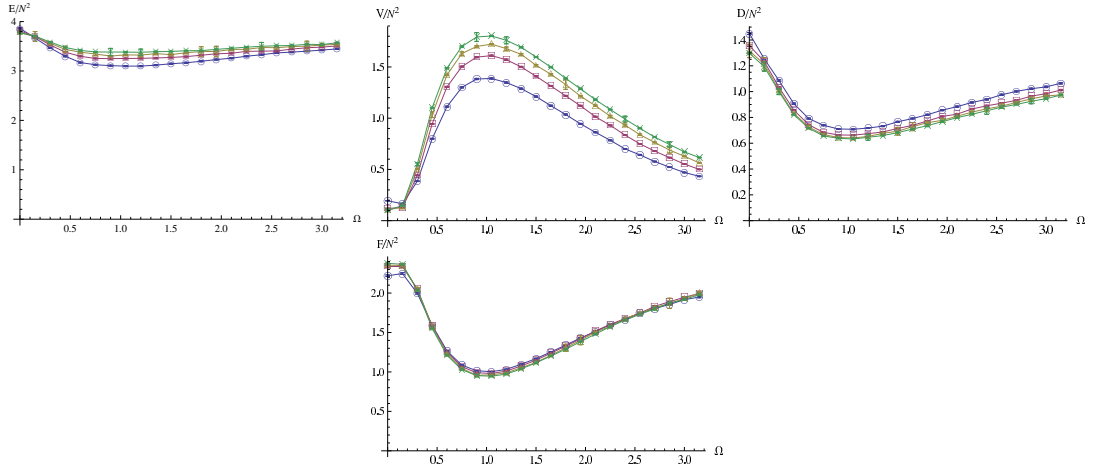
11

Figure 4: Total energy density and the various contributions for $\mu = 1$, $\alpha = 0$ varying Ω and N. From the left to the right E, V, D, F with $N = 5$ (circle), $N = 10$ (square), $N = 15$ (triangle), $N = 20$ (cross).
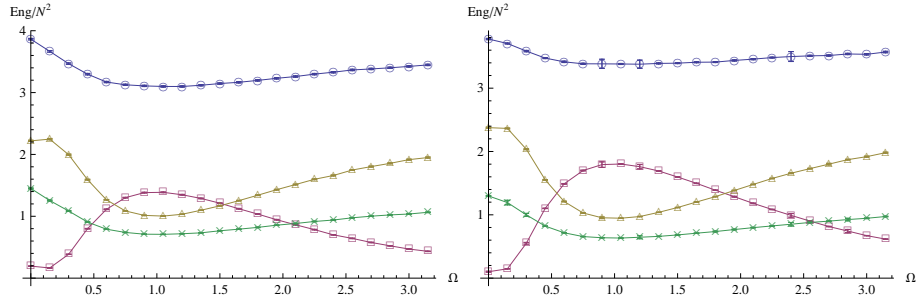

Figure 5: Comparison of the total energy density and the various contributions for $\mu = 1$, $\alpha = 0$. E (circle), F (triangle), D (cross), V (square). With $N = 5$ (left) and $N = 20$ (right).

The specific heat density in fig.6 shows a small peak in $\Omega = 0$. This peak does not increases as N increases, therefore is not related to a phase transition.
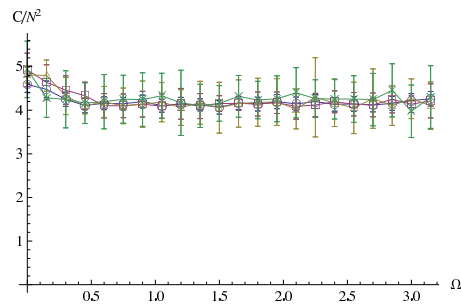
Figure 6: Specific heat for $\mu = 1$.

In order to gain some information on the composition of the fields we look at the order parameters defined in the previous section. Starting from the scalar field ψ, fig.7 shows the

plots for $\langle\varphi_a^2\rangle$, $\langle\varphi_0^2\rangle$ and $\langle\varphi_1^2\rangle$ for $N = 5$. The three values $\langle\varphi_a^2\rangle$, $\langle\varphi_0^2\rangle$ and $\langle\varphi_1^2\rangle$ seem essentially constant, where the spherical contribution $\langle\varphi_0^2\rangle$ to the full-power-of-the-field is dominant. The
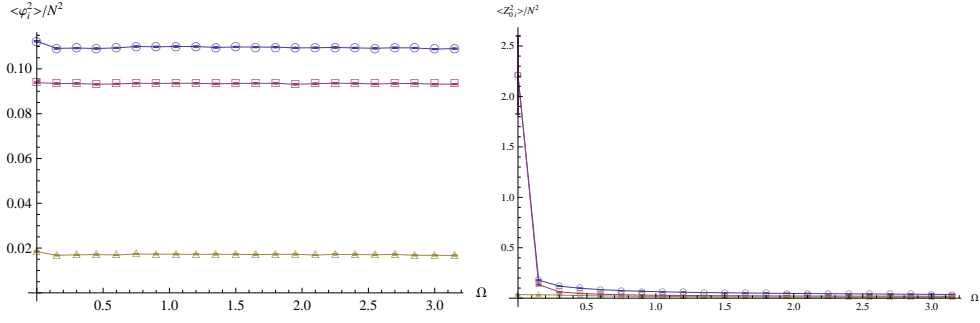
Figure 7: On the left comparison of $\langle\varphi_a^2\rangle$ (circle), $\langle\varphi_0^2\rangle$ (square) and $\langle\varphi_1^2\rangle$ (triangle) density. On the right comparison of $\langle Z_{0a}^2\rangle$ (circle), $\langle Z_{00}^2\rangle$ (square) and $\langle Z_{01}^2\rangle$ (triangle) density.

behaviour of the Z_0 fields (which describe the covariuant coordinates) is different. Here the spherical contribution becomes dominant only for Ω approaching 0, starting from a zone in which the contribution of $\langle Z_{00}^2\rangle$ and $\langle Z_{01}^2\rangle$ are comparable. For brevity we only show the plots for $\langle Z_{0a}^2\rangle$, $\langle Z_{00}^2\rangle$ and $\langle Z_{01}^2\rangle$, but taking into account the statistical errors, the other Z_i-related plots are compatible to the Z_0-case. The dependence of the previous quantities on N is shown in the following plots fig.8. All previous parameters decrease with N, but the dominance of φ_0
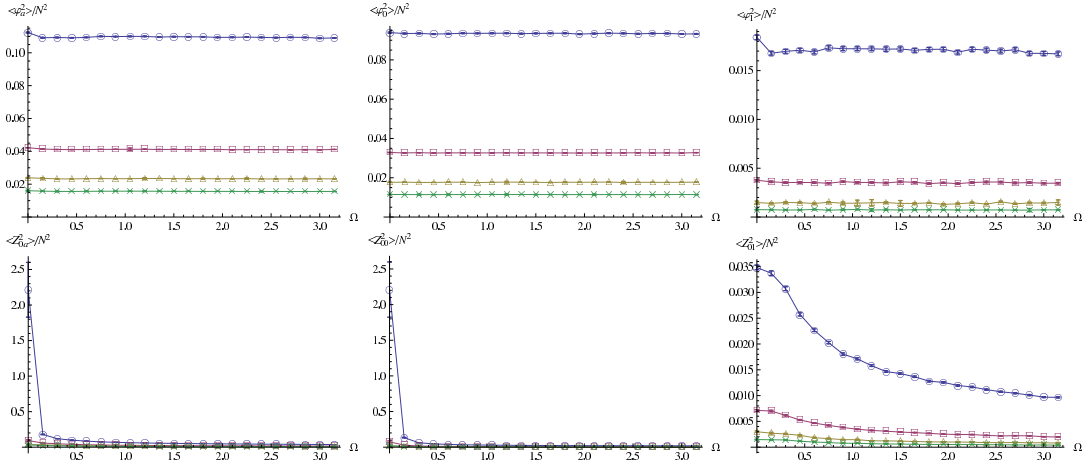
Figure 8: Starting from the up left corner and from the left to the right the densities for $\langle\varphi_a^2\rangle$, $\langle\varphi_0^2\rangle$, $\langle\varphi_1^2\rangle$, Z_{0a}^2, $\langle Z_{00}^2\rangle$ and $\langle Z_{01}^2\rangle$ for $\mu = 1$ varying Ω and N.

on the total-power-of-the-field is independent by N. The peak related to Z_0 decreases with N, but if we look at the single plot for the spherical contribution at $N = 20$, the peak persists as Ω approaches $\Omega = 0$.

Now we will analyse the model for $\mu = 0$. Fig.9 shows the plots for total energy density and the contributions V, D, F. The slope of the total energy density seems to be constant. The D-contribution and the F-contribution do not balance each other like in the previous case, but all three contributions balance themselves to produce a constant sum.
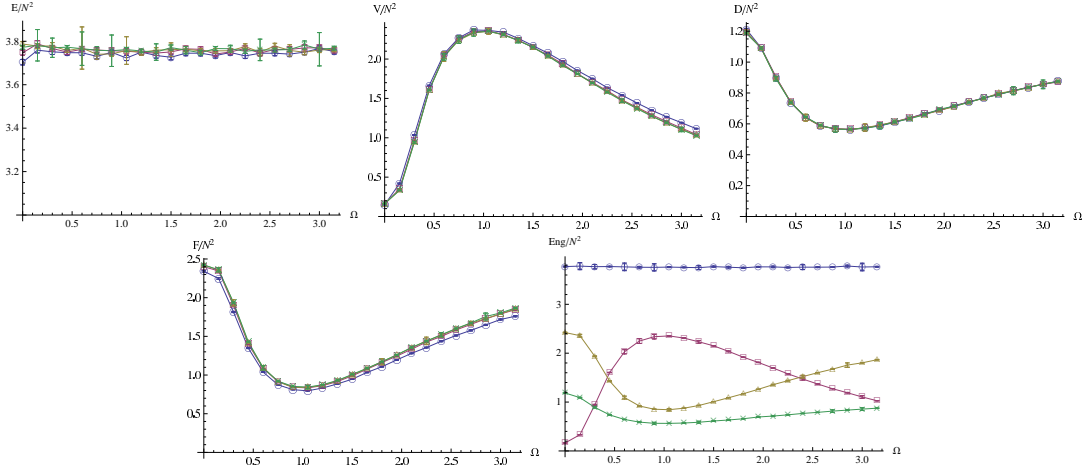
13

Figure 9: Total energy density, various contributions and the comparison among them for $\mu = 0$ varying Ω and N. From the left to the right E, V, D, F and comparison.

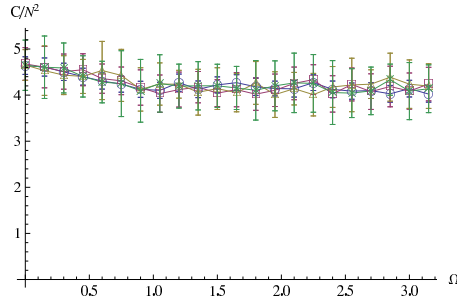The specific heat density fig.10 shows again the small peak in $\Omega = 0$ without N-dependence.

Figure 10: Specific heat density for $\mu = 0$ varying Ω and N.

For the other quantities $\langle\varphi_a^2\rangle$, $\langle\varphi_0^2\rangle$, $\langle\varphi_1^2\rangle$ and $\langle Z_{0a}^2\rangle$, $\langle Z_{00}^2\rangle$, $\langle Z_{01}^2\rangle$ we have according to fig.11 the same behaviour as in the case $\mu = 1$.

A completely different response of the system is obtained in the plots for $\mu = 3$, as we can see from fig.12. The slope of total energy density is very similar to the F-component instead of D. However, there appears a sharp minimum around $\Omega = 0.1$ and two maxima at $\Omega \approx 0.6$ and $\Omega \approx 1.8$ for large N. This dramatic change in the plots might be interpreted as consequence of a phase transition in the parameter μ. Actually, in the next section we will find a peak in the specific heat density for some fixed Ω and varying $\mu \in [0, 3]$.

The specific heat density fig.13 displays a strong change, too. In fact, instead of the peak at $\Omega = 0$, the peak appears close to the origin around $\Omega = 0.15$. This peak, in contrast to the previous ones, grows as N increases and therefore could indicate a phase transition.

The fig.14 describes the behaviour of the order parameters densities $\langle\varphi_a^2\rangle$, $\langle\varphi_0^2\rangle$, $\langle\varphi_1^2\rangle$ and $\langle Z_{0a}^2\rangle$, $\langle Z_{00}^2\rangle$, $\langle Z_{01}^2\rangle$. They show a similar behaviour as the corresponding plots for $\mu = 1$ and $\mu = 0$. For the ψ field the spherical contribution remains dominant. However, in the $\langle\varphi_1^2\rangle$ plot
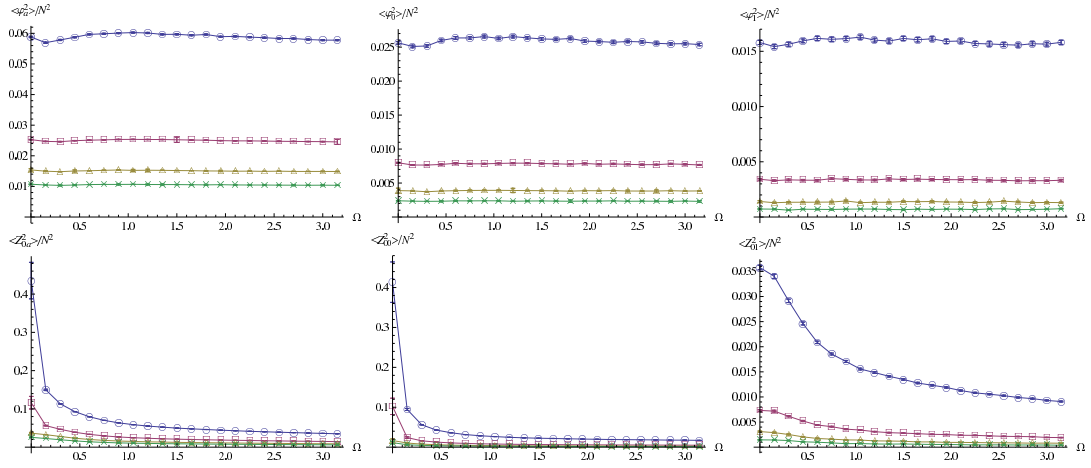
14

Figure 11: Starting from the up left corner and from the left to the right the densities for $\langle\varphi_a^2\rangle$, $\langle\varphi_0^2\rangle$, $\langle\varphi_1^2\rangle$, $\langle Z_{0a}^2\rangle$, $\langle Z_{00}^2\rangle$ and $\langle Z_{01}^2\rangle$ for $\mu=0$ varying Ω and N.
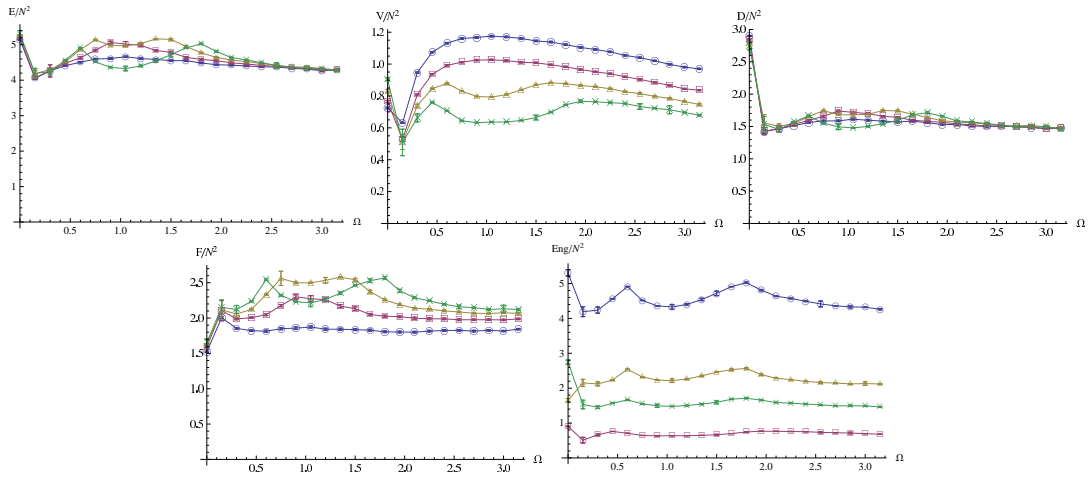

Figure 12: Total energy density, various contributions and the comparison among them for $\mu=3$ varying Ω and N. From the left to the right E, V, D, F and comparison.

there appears a deviation from the constant slope. This deviation is evident for $N=5$ but still present for higher N. The order parameters for Z_0 display a peak close to the origin without oscillations even for $N=5$. This maximum for higher N does not move closer to the origin, in other words, this shift is not caused by finite volume effects. Even for Z_{01}^2 there appears a peak at $\Omega=0$ which becomes shifted and smoother for higher N.

5.3 Varying μ

In this section we analyse the response of the system varying $\mu \in [0,3]$ while Ω is fixed at 0, 1 or 3, and α is always zero. We start displaying the plots fig.15 of the total energy density and of various contributions for $\Omega=0$. There is no evident discontinuity but there appears a peak in the total energy density around $\mu \approx 2.5$ for $N=20$. Comparing all the contributions it is easy
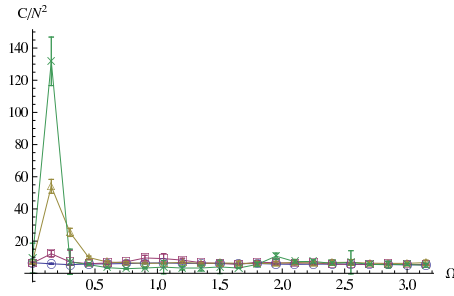
15

Figure 13: Specific heat density for $\mu = 3$ varying Ω and N.

to notice that the slope of the total energy is dictated by the curve V of the potential part.

As mentioned before, the specific heat density fig.16 features a peak around $\mu \approx 2.5$ for $N = 20$. Again, since the peak increases with N, we could relate this to a phase transition. The plots for the quantities $\langle \varphi_a^2 \rangle$ and $\langle \varphi_0^2 \rangle$ show a strong dependence on μ, in particular the slope of $\langle \varphi_0^2 \rangle$ seems mostly linear. The plot for $\langle \varphi_1^2 \rangle$ also increases with μ, but not linearly. From the first three plots of fig.17 we deduce that close to the origin the non-spherical contribution $\langle \varphi_1^2 \rangle$ is bigger than the spherical one $\langle \varphi_0^2 \rangle$. Increasing μ, this situation capsizes and $\langle \varphi_0^2 \rangle$ becomes dominant over $\langle \varphi_1^2 \rangle$.

The behaviour of the Z_0 fields as shown in the last three plots of fig.17 is quite different. The spherical contribution is always dominant for the whole interval $\mu \in [0, 3]$. The curves for $\langle Z_{0a}^2 \rangle$, $\langle Z_{00}^2 \rangle$ are compatible to the constant slope. For $\langle Z_{01}^2 \rangle$ we have the same dependence on μ, in particular there is a smooth descending step which becomes smoother for bigger N. However, we admit that due to some cancellation effects, the statistical errors are quite big so that this interpretation is not fully conclusive. Anyway, this result demonstrates the dependence of the order parameter for Z_i, and in general of the system, on the two choices $\Omega = 0$ or $\Omega \neq 0$.

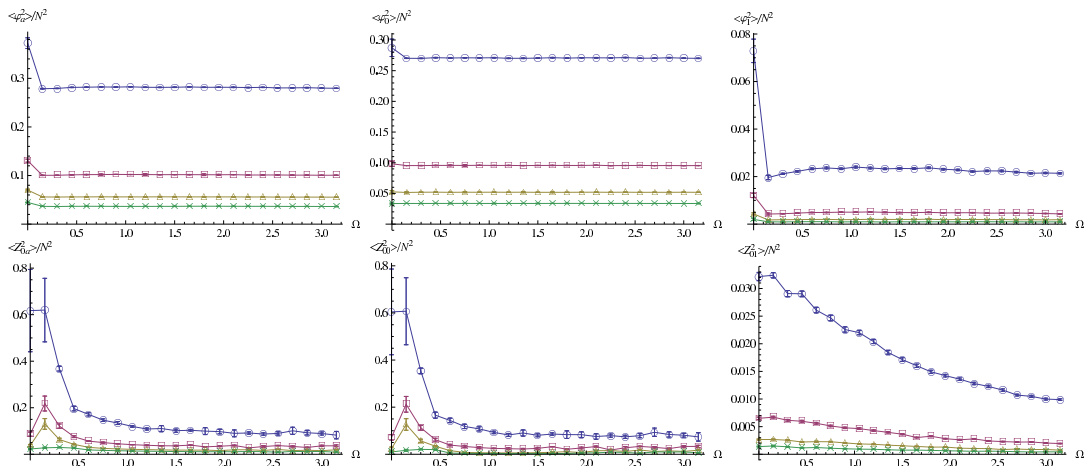Now we will analyse the model for $\Omega = 1$. As fig.18 shows, the plots have a different slope

Figure 14: Starting from the up left corner and from the left to the right the densities for $\langle \varphi_a^2 \rangle$, $\langle \varphi_0^2 \rangle$, $\langle \varphi_1^2 \rangle$, $\langle Z_{0a}^2 \rangle$, $\langle Z_{00}^2 \rangle$ and $\langle Z_{01}^2 \rangle$ for $\mu = 3$ varying Ω and N.
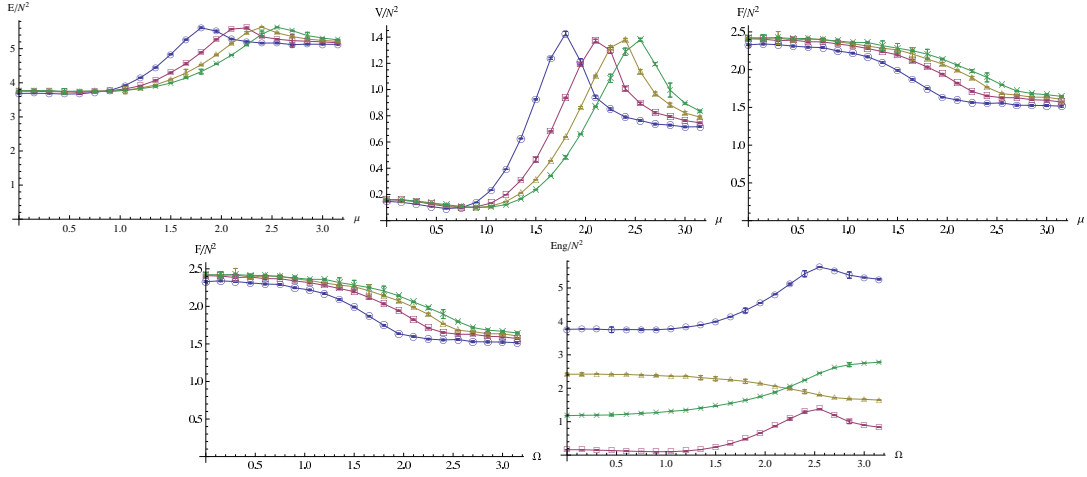
16

Figure 15: The total energy density and the various contributions for $\Omega = 0$ varying μ and N. From the left to the right E, V, D, F an comparison with $N = 5$ (circle), $N = 10$ (square), $N = 15$ (triangle), $N = 20$ (cross). For the comparison: E (circle), V (square), D (triangle), F (cross).
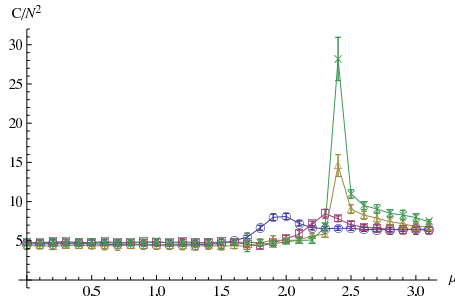

Figure 16: Specific heat density for $\Omega = 0$ varying μ and N.

compared to the previous case. The maximum of total energy density follows the one of the V-component. If we focus only on the total energy plot and compare it with the one for $\Omega = 0$, we notice a shift of the maximum for each N. In particular, in fig.18 some maxima are moved outside the considered interval. We can find this shift very clearly looking at specific heat density plotted in fig.19. Here again the peak both increases with N and is shifted to $\mu \approx 3.3$.

Fig.20 shows for $\langle \varphi_a^2 \rangle$, $\langle \varphi_0^2 \rangle$ the same behaviour as in the case $\Omega = 0$. The plot for $\langle \varphi_1^2 \rangle$ displays an almost constant curve. However, close to the origin, the spherical contribution and the first non-spherical one are comparable. The introduction of $\Omega \neq 0$ creates, in the Z_0-order parameters shown in fig.20, a dependence similar to the plots for ψ. The full-power-of-the-field density and the spherical contribution are no longer constant, they grow as μ increases. Even in this case the spherical contribution is always dominant excluding the region around $\mu = 0$.

The last set of plots treats the case $\Omega = 3$. The following diagrams for the energy and its contributions show the absence of the previous peak. They show a sort of dilatation of the former plots of fig.18.

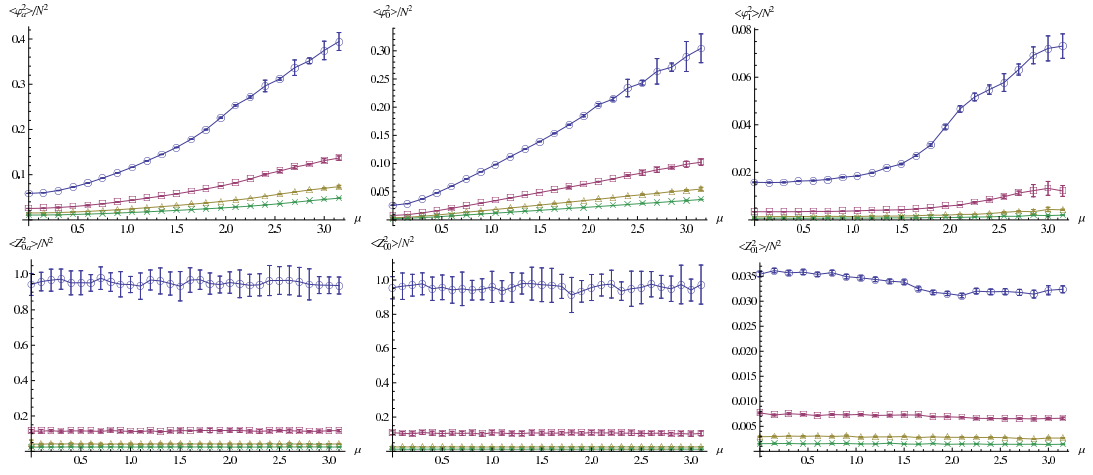The specific heat density fig.22 does not show the peak in zero anymore, and the curves do

Figure 17: Starting from the up left corner and from the left to the right the densities for $\langle \varphi_a^2 \rangle$, $\langle \varphi_0^2 \rangle$, $\langle \varphi_1^2 \rangle$, $\langle Z_{0a}^2 \rangle$, $\langle Z_{00}^2 \rangle$ and $\langle Z_{01}^2 \rangle$ for $\Omega = 0$ varying μ and N.
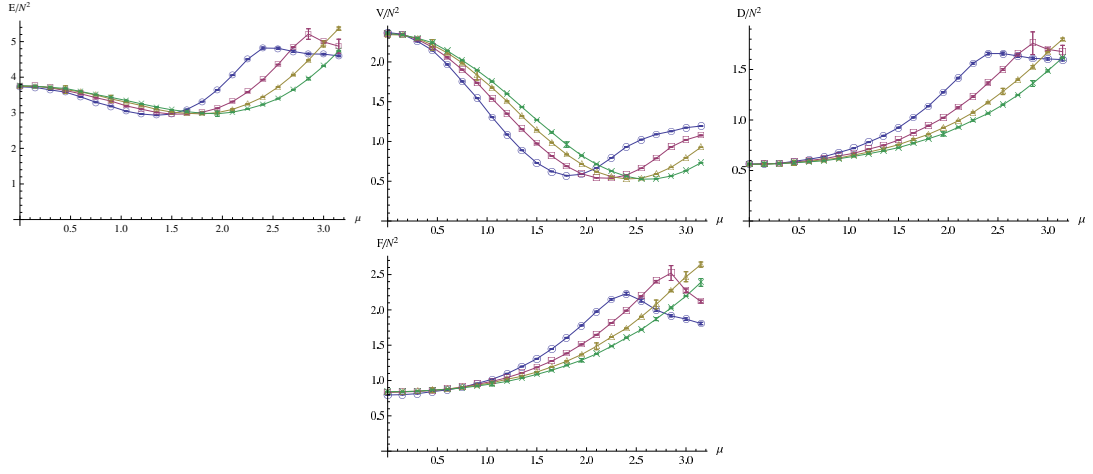

Figure 18: Total energy density and contributions for $\Omega = 1$ varying μ and N. From the left to the right E, V, D, F.
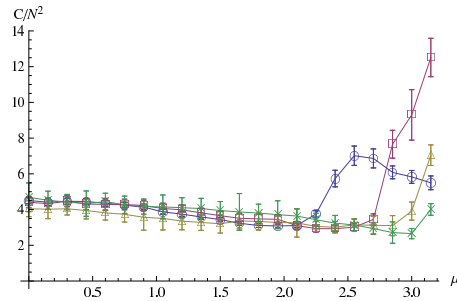

Figure 19: Specific heat density for $\Omega = 1$ varying μ and N.
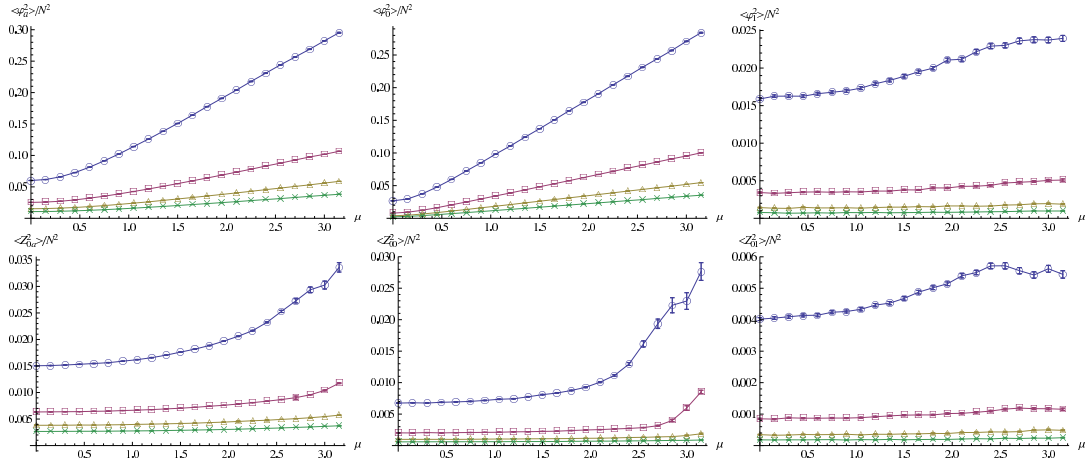
18

Figure 20: Starting from the up left corner and from the left to the right the densities for $\langle \varphi_a^2 \rangle$, $\langle \varphi_0^2 \rangle$, $\langle \varphi_1^2 \rangle$, $\langle Z_{0a}^2 \rangle$, $\langle Z_{00}^2 \rangle$ and $\langle Z_{01}^2 \rangle$ for $\Omega = 1$ varying μ and N.
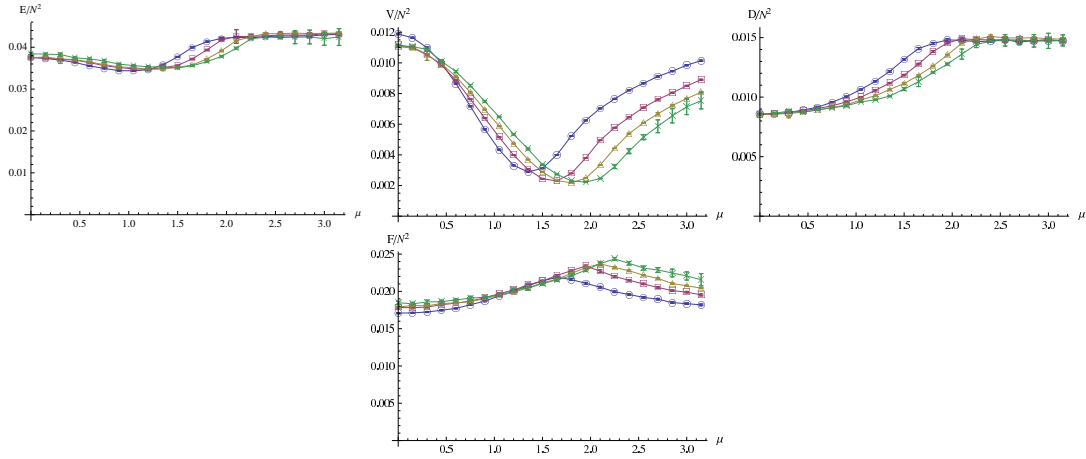

Figure 21: Total energy density and the various contributions for $\Omega = 3$ varying μ and N. From the left to the right E, V, D,F .

not show any particular point as N increases. Actually, the peak can be found for higher μ.

At last in fig.23 we find a behaviour of the density of the order parameters for the Z_0 and ψ fields similar to the former plots for $\Omega = 1$, and they are compatible with a dilatation of the previous plots.

Conclusions and prospectives

We have studied a noncommutative gauge theory which arises by restriction of the spectral action for harmonic Moyal space to finite matrices. For this quantum field theoretical model we have performed Monte Carlo simulations to obtain, as function of the parameters (μ, Ω), non-perturbative information for the energy density, for various contributions to the energy
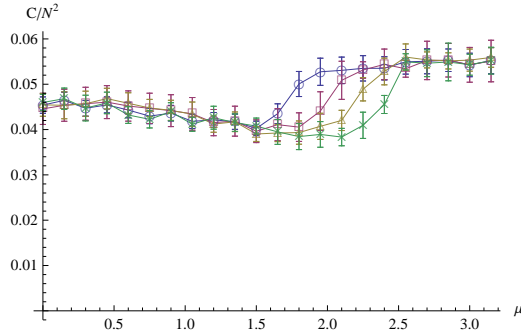
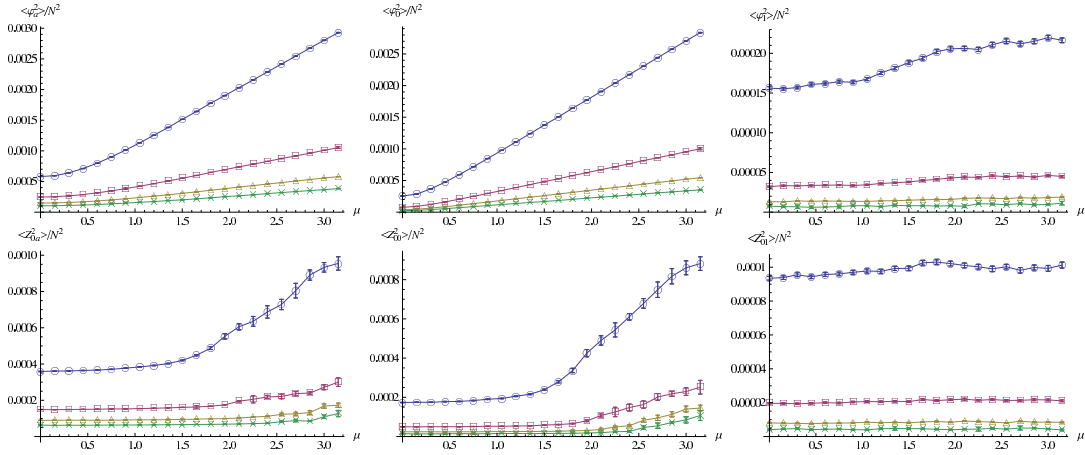Figure 22: Specific heat density for $\Omega = 3$ varying μ and N.

Figure 23: Starting from the up left corner and from the left to the right the densities for $\langle \varphi_a^2 \rangle$, $\langle \varphi_0^2 \rangle$, $\langle \varphi_1^2 \rangle$, $\langle Z_{0a}^2 \rangle$, $\langle Z_{00}^2 \rangle$ and $\langle Z_{01}^2 \rangle$ for $\Omega = 3$ varying μ and N.

density and for the specific heat density, as well as for a set of order parameters related to sphericity. Despite the complexity of the approximated spectral action considered here, we were able to obtain some reliable numerical results, showing that a numerical treatment of this kind of noncommutative gauge models seems feasible. However, as the restriction to finite matrices shows severe differences to the original smooth action, the relevance of our results to the smooth case is not clear.

The specific heat density shows various peaks which could indicate phase transitions. In particular, studying the behaviour for some fixed mass parameter μ we found a relevant peak close to $\Omega = 0$ for $\mu = 3$, and we noticed a big change in the energy density and in its contributions between the cases $\mu \in \{0, 1\}$ and $\mu = 3$. Other peaks in the specific heat density can be found varying μ and fixing Ω. The plots show that increasing Ω, the peak in the specific heat which starts at $\mu \approx 2.4$ for $\Omega = 0$ is moved towards higher μ. The order parameters we introduced show a strong dependence on the cases $\Omega = 0$ versus $\Omega \neq 0$. Referring to the fixed-μ plots we found a peak in the spherical contribution for the gauge fields Z_i. Its behaviour can be interpreted as a sort of symmetry breaking introduced by $\Omega \neq 0$. Additionally, varying μ and fixing Ω, the other parameters display a slope increasing with μ for all fields and all situations

20

but one: the plots of the order parameters $\langle Z_{0a} \rangle$, $\langle Z_{00} \rangle$ for $\Omega = 0$ show a constant behaviour.

The natural next steps in the numerical study of this model could be the computation of the transition curves in order to separate the phase regions and to classify them using possibly additional order parameters. Our treatment, forced by limited resource, was conducted varying Ω in the range $[0, 3.1]$, since the Langmann-Szabo duality does not hold anymore in our case. Actually, the computed plots do not show any periodicity in $\Omega \in [0, 1]$ so that we can infer that in contrast to the scalar case the range $[0, 1]$ is not enough to describe the system.

It will be very interesting to relax the condition $\mu^2 > 0$. Implementing $\mu^2 < 0$ amounts to conduct the calculation no longer around the minimum of the action, in particular avoiding the explicit use of the finite vacuum and considering directly the four indexed components we can hope in some improvement in the behavior of the large N limit making the simulations much more harder (but not impossible), however the limit can continue to show big differences. Such continuous limit issues are not new for the simulations of a scalar field theory on matrix model, in facts in [28, 29] is discovered a so-called matrix phase, which is not present in the continuous model, as a result the infinite matrix limit fails to converge to the classical case. The adding of an extra term to the matrix action [30] solves the problem making the new anomalous phase transition to disappear. The extension of the parameters space, together with the classification of the different phase regions, would allow us to compare our model with the results of the simulation performed for the fuzzy sphere, have a look at the occurrence of a correspondent matrix phase and eventually to try to regularize the infinite matrix limit.

Acknowledgements

References

[1] M. R. Douglas, "Two lectures on D-geometry and noncommutative geometry," in: *Nonperturbative aspects of strings, branes and supersymmetry*, eds M. Duff et al, World Scientific Singapore (1999) 131–156 [hep-th/9901146].

[2] R. J. Szabo, "Quantum field theory on noncommutative spaces," Phys. Rept. **378** (2003) 207–299 [hep-th/0109162].

[3] R. Wulkenhaar, "Field Theories On Deformed Spaces," J. Geom. Phys. **56** (2006) 108–141.

[4] J. M. Gracia-Bondia, J. C. Varilly, "Algebras of distributions suitable for phase space quantum mechanics. I.," J. Math. Phys. **29** (1988) 869–879.

[5] J. Madore, "The fuzzy sphere," *Class. Quant. Grav.* **9** (1992) 69–88.

[6] S. Minwalla, M. Van Raamsdonk and N. Seiberg, "Noncommutative perturbative dynamics," JHEP **0002** (2000) 020 [arXiv:hep-th/9912072].

[7] H. Grosse and R. Wulkenhaar, "Renormalisation of ϕ^4-theory on noncommutative $\mathbb{R}^4$ in the matrix base," Commun. Math. Phys. **256** (2005) 305–374 [arXiv:hep-th/0401128].

[8] H. Grosse and R. Wulkenhaar, "Renormalisation of ϕ^4-theory on non-commutative $\mathbb{R}^4$ to all orders," Lett. Math. Phys. **71** (2005) 13–26 [arXiv:hep-th/0403232].

[9] V. Rivasseau, F. Vignes-Tourneret and R. Wulkenhaar, "Renormalization of noncommutative ϕ^4-theory by multi-scale analysis," Commun. Math. Phys. **262** (2006) 565–594 [arXiv:hep-th/0501036].

[10] R. Gurau, J. Magnen, V. Rivasseau and F. Vignes-Tourneret, "Renormalization of noncommutative ϕ_4^4 field theory in x-space," Commun. Math. Phys. **267** (2006) 515–542 [arXiv:hep-th/0512271].

[11] R. Gurau and V. Rivasseau, "Parametric representation of noncommutative field theory," Commun. Math. Phys. **272** (2007) 811–835 [arXiv:math-ph/0606030].

[12] V. Rivasseau, "Non-commutative renormalization," in *Quantum spaces*, Prog. Math. Phys. **53** (2007), Birkhäuser, Basel [arXiv:0705.0705 [hep-th]].

[13] E. Langmann and R. J. Szabo, "Duality in scalar field theory on noncommutative phase spaces," Phys. Lett. B **533** (2002) 168–177 [arXiv:hep-th/0202039].

[14] A. Matusis, L. Susskind and N. Toumbas, "The IR/UV connection in the non-commutative gauge theories," JHEP **0012** (2000) 002 [arXiv:hep-th/0002075].

[15] A. Connes, *Noncommutative Geometry*, Academic Press, Inc. (1994).

[16] A. H. Chamseddine and A. Connes, "The spectral action principle," Commun. Math. Phys. **186** (1997) 731–750 [arXiv:hep-th/9606001].

[17] V. Gayral, J. M. Gracia-Bondía, B. Iochum, T. Schücker and J. C. Várilly, "Moyal planes are spectral triples," Commun. Math. Phys. **246** (2004) 569–623 [arXiv:hep-th/0307241].

[18] V. Gayral and B. Iochum, "The spectral action for Moyal planes," J. Math. Phys. **46** (2005) 043503 [arXiv:hep-th/0402147].

[19] A. de Goursac, J. C. Wallet and R. Wulkenhaar, "Noncommutative induced gauge theory," Eur. Phys. J. C **51** (2007) 977–987 [arXiv:hep-th/0703075].

[20] H. Grosse and M. Wohlgenannt, "Induced Gauge Theory on a Noncommutative Space," Eur. Phys. J. **C52** (2007) 435–450 [arXiv:hep-th/0703169].

[21] H. Grosse and R. Wulkenhaar, "8D-spectral triple on 4D-Moyal space and the vacuum of noncommutative gauge theory," arXiv:0709.0095 [hep-th].

[22] R. Wulkenhaar, "Non-compact spectral triples with finite volume," in: *Quanta of Maths*, Clay Math. Proc. **11** (2010) 617, Amer. Math. Soc., Providence, RI [arXiv:0907.1351 [hep-th]].

[23] V. Gayral and R. Wulkenhaar, "Spectral geometry of the Moyal plane with harmonic propagation," arXiv:1108.2184 [math.OA].

[24] A. de Goursac, J.-C. Wallet and R. Wulkenhaar, "On the vacuum states for noncommutative gauge theory," Eur. Phys. J. C **56** (2008) 293–304 [arXiv:0803.3035 [hep-th]].

[25] I. Montvay and G. Münster, *Quantum Field Theory on a Lattice*, Cambridge University Press, (1997).

[26] M. E. Newman and G. T. Barkema, *Monte Carlo Methods in Statistical Physics*, Oxford University Press (2002).

[27] A. Connes, J. Lott, "Particle Models And Noncommutative Geometry (expanded Version)," Nucl. Phys. Proc. Suppl. **18B** (1991) 29–47.

[28] X. Martin, "A matrix phase for the ϕ^4 scalar field on the fuzzy sphere," JHEP 0404 (2004) 077 [hep-th/0402230].

[29] J. Medina, "Fuzzy Scalar Field Theories: Numerical and Analytical Investigations," arXiv:0801.1284v1 [hep-th].

[30] J. B.P. Dolan, D. OConnor and P.Prenajder, "Matrix φ^4 Models on the Fuzzy Sphere and their Continuum Limits," JHEP 0203 013 (2002).

[31] B. Spisso, "A numerical approach to harmonic non-commutative spectral field theory," PhD thesis arXiv:1111.2871v1 [math-ph].

[32] B. Spisso, "First numerical approach to a Grosse-Wulkenhaar model," Contribution to the proceedings of the EU-NCG 4th Annual Meeting arXiv:1111.2951v1 [hep-th].

[33] M. Panero, "Quantum field theory in a non-commutative space: Theoretical predictions and numerical results on the fuzzy sphere," SIGMA 2 (2006) 081 [arXiv:hep-th/0609205].

[34] M. Panero, "Numerical simulations of a non-commutative theory: The Scalar model on the fuzzy sphere," JHEP 0705 (2007) 082 [arXiv:hep-th/0608202].